ELSEVIER

Journal of Nuclear Materials 303 (2002) 147–155

journal of nuclear materials

www.elsevier.com/locate/jnucmat

X-ray measurement of near surface residual stress in textured cold-worked stress-relieved Zr–2.5%Nb pressure tube material

K. Kapoor *, D. Lahiri, C. Padmaprabu, T. Sanyal

Advanced Materials Characterizations Laboratory, Nuclear Fuel Complex, Hyderabad 500 062, India

Received 17 December 2001; accepted 5 March 2002

Abstract

In the present study, the near surface residual stress in Zr–2.5%Nb pressure tubes was measured using X-ray diffraction. Both cold rolled (pilgered) and stress-relieved tubes were studied. Since the material is highly textured and the hexagonal close packed crystal lattice has anisotropic elastic constants, special care is required in collection and analysis of experimental data to minimise errors. The standard multi-exposure technique of X-ray residual-stress measurement results in inaccuracies for textured material. Diffraction intensities depend on factors like inclination of the sample, the rotation of the beam and the position of detectors. Low intensity due to texture can result in increased uncertainties in observed stress value. Anisotropy of elastic constants in textured materials can further increase the errors in measured stress. A general approach has been developed for accurate determination of the stress tensor in textured material. The measured stresses for Zr–2.5%Nb pressure tubes were highest and compressive along the rolling direction (RD) in the pilgered samples. The stress-relieved samples showed a small tensile component along the RD. Errors up to 20% are introduced if isotropic elastic constants are used in the analysis instead of the more realistic anisotropic elastic constants calculated for the observed texture.

1. Introduction

Pressurized Heavy Water Reactors (PHWR) use zirconium base alloys due to their low neutron absorption cross-section, good elevated temperature mechanical strength, low irradiation creep and high corrosion resistance in reactor atmosphere. Zr–2.5wt%Nb alloy (hereafter called Zr–2.5Nb), currently used for pressure tubes, has replaced Zircaloy-2 due to its better physical and mechanical properties leading to increased life in the reactor. High residual stresses are generated in fabricated components of Zr–2.5Nb alloy during mechanical and thermal treatments because of highly anisotropic hexagonal closed packed (HCP) structure of the zirconium. These stresses play an important role in subsequent deformation and help in determining the radiation stability of the reactor core components. Harde and Shanahan [1] found that residual stresses have a pronounced effect on hydride reorientation in Zr–2.5Nb tube material. Residual stress variation with depth leads to zoning of hydrides, i.e., separate zones of differently oriented hydrides are formed through the thickness depending on the periodic variation of stress (tensile and compressive). Since hydrides are brittle in nature, they can get reoriented at stress concentration regions like roll joints and initiate cracking. The characterization of residual stress is thus very important for Zr–2.5Nb nuclear reactor components. X-ray residual stress measurement method is used to characterize Zr–2.5Nb samples.

The surface residual stresses are usually measured using the multi-exposure side-inclination technique. In this technique the peak mid position is measured by curve fitting (Gaussian/Pearson IV). The shift in the peak position is determined as a function of change in

* Corresponding author. Tel.: +91-40 712 0151x4091; fax: +91-40 712 1209.

E-mail address: kapoork@nfc.ernet.in (K. Kapoor).

0022-3115/02/$ - see front matter
PII: S0022-3115(02)00818-8

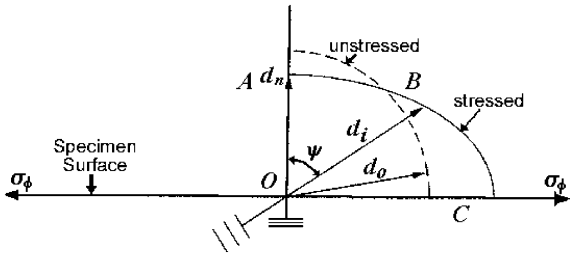

Fig. 1. Vector diagram indicating variation of lattice spacing d with change in inclination angle for stressed and stress free conditions.

inclination angles (Fig. 1). The residual stress is determined using the following relationship:

$$\sigma_\phi = -\{(E/2)(1+\nu)\}\cot\theta d(\Delta 2\theta)/d(\sin^2\Psi), \quad (1)$$

where σ_ϕ is the stress in the direction ϕ, E is elastic modulus and ν is poisson's ratio, Ψ is the inclination angle measured in direction ϕ and θ is the Bragg's diffraction angle and $\Delta 2\theta$ is the shift in the Bragg's angle due to change in lattice spacing measured at given Ψ and ϕ.

These stresses are then measured in the three rotation angles using bulk elastic constants and then principal stresses are determined.

For the isotropic materials the 'crystal lattice spacing (d)' varies linearly with '$\sin^2\psi$' (ψ is the inclination angle of the X-ray), whereas, in the case of textured materials like zirconium-based alloys, the variation is non-linear. This is due to the anisotropy of the material including elastic constants and the broader diffraction peaks with low intensity. In 1975, Marion and Cohen [2] first tried to correct these texture induced curvature with the aid of the crystal concentration data obtained from pole figures. Their method assumes a biaxial stress field with an additional dependence of lattice spacing on the texture distribution function $f(\psi)$, a measure of the (hkl) pole density calculated from diffracted intensity over the range of ψ tilts used for stress measurement. The model assumes a lattice spacing dependence of

$$d_{\psi\phi} = \{(1+\nu)/E\}_{(hkl)}\sigma_\phi d_o \sin^2\psi + (d_{\max} - d_B)f(\psi) + d_B, \quad (2)$$

where ϕ is the angle of rotation,$\psi$is angle of inclination, $d_{\psi\phi}$ is lattice spacing for given ϕ- and ψ- values, $d_{\max}$ and d_B are maximum and minimum lattice spacings in the range investigated, E is Young's modulus, ν is Poisson's ratio, (hkl) is crystallographic plane for which d is measured and σ_ϕ is residual stress in ϕ direction.

This method requires simultaneous determination of the preferred orientation, or texture $f(\psi)$, in the sample along with the lattice spacing. This is solved by multiple linear regression over the functions $f(\psi)$ and $d_{\psi\phi}$ as a functions of $\sin^2\psi$ to determine d_ϕ, $d_{\max}$ and d_B.

Hauk and Sesemann [3] found that in steels two texture independent directions occur in which the lattice strain is isotropic or quasi-isotropic. These two ψ-values were used to get linear relationship between the strain and $\sin^2\psi$. Methods described in references [2] and [3] assume a quasi-isotropic system whereby, the elastic interaction or coupling between the grains and its surrounding matrix is not considered [4].

In a study by Gazzara [4] direct experimental method were used to correct the X-ray residual stress measurements for the effect of texture in rolled steel plates. A series of intensity and 2θ vs. $\sin^2\psi$ plots were made, over the range of $\psi_{0,\alpha}$ angles for constant α-values. The first four plots showed a non-linear relationship between $\sin^2\psi$ and 2θ or d while the plot at $\alpha = 42°$ showed a linear relationship. It was concluded that a texture independent path is achieved for the side inclining case ($\alpha = 42°$) for (2 1 1) reflections. Correct values of residual stress could be achieved at this particular side inclination by using the d-spacing at $\alpha = 42°$ with stress free sample as the d_o. But, in this study, the directional elastic constants were not been calculated for measuring residual stress, though the material was textured. Probably, as this material was cubic, the effect may not be significant.

In case of evaluation of residual stress in textured cubic material (low carbon steel) by Dolle and Cohen [5] six anisotropic elastic constants were found by calculation. These were found through interpretation of actual texture in terms of ideal components. Results show a quantitative agreement with the observed oscillation to steel in (2 1 1) reflection by CrK_α radiation. It has also been shown that X-ray elastic constant for {h 0 0} and {h h h} reflections are independent of ϕ and ψ in case of cubic materials. Measurement done on (2 0 0) and (2 1 1) plane with three directions, RD, 60° to RD and TD, shows linear relation between lattice strain and $\sin^2\psi$ excepting the reflection from (2 1 1) plane in RD. It is further mentioned that the similar type of quasi-isotropic plane in hexagonal system is {0 0 0 h} set of planes. But, this limits the measurement with only one set of planes, which is not always a viable option.

Residual stress in Zircaloy-2 with rod texture was calculated by Turner and Tome [6] and by MacEwen and Tome [7] using 'elasto-plastic self-consistence model (EPSC)' [8,9], which accounts for grain interaction. Their results were in good quantitative agreement with experimental determination of residual strain obtained by neutron diffraction. The EPSC model was used by Pang et. al. [10] for analysis of residual stress in uniaxial and biaxial tension loading condition of Zircaloy-2 with rod texture.

In 1989, MacEwen et al. [11] used 'QUEST', a polycrystalline deformation model, for calculating the

residual stress in annealed Zircaloy. This model accounts for anisotropic elasticity, plasticity, thermal expansion and crystallographic texture of the samples. The input requires texture data of the sample in terms of number of grain orientation together with corresponding weights. But this model assumes no plastic relaxation in the material and there is 10% difference between the predicted and experimental results.

According to MacEwen et al. [12], interpretation of the diffraction data is greatly simplified by sharp axisymmetric texture in the material, like rod texture in Zircaloy-2. In idealized rod texture every grain has its basal pole orthogonal to the axis of the rod. Since α-Zr is almost isotropic plastically in the basal plane, the variation of residual strain from grain to grain within a given subset will be small. Thus, the data can be interpreted in terms of the residual stress state in a single orientation of grains. Reasonable agreement was observed between prediction based on Taylor's analysis following this approach and experimental measurements. The exact texture of the material in the study is not well illustrated to effectively describe the effect of texture.

Sue [13] measured the X-ray elastic constants for (4 2 2) and (3 3 3)/(5 1 1) reflections of the {1 1 1} textured TiN coating exhibiting high elastic anisotropy. X-ray elastic constants varied significantly with crystallographic orientation. The residual stresses for both the reflections of TiN, which were determined by '$\sin^2\psi$' method, with measured X-ray elastic constants were in good comparison with the RS values determined by bimetal reflection technique.

As seen above direct application of Eq. (1) in a textured material leads to errors. In our study on textured material we have adopted an approach where residual stress measurement is done along some texture independent paths. Texture independent path is an angular inclination in the measuring direction with respect to the sample co-ordinate system for which intensity of the peaks will be same in the two detectors for all the ψ tilts of the beam.

In the present study we have determined the correct inclination angles leading to texture independent measurement paths for calculation of residual stress and the three stress measurement directions (required for principal stress). This was obtained by superimposing the Wulff net on (10.3) pole figure and choosing the proper inclination angles having good intensity peaks. Zarakades and Larson [14] established that moderately accurate predictions of elastic anisotropy can be made for polycrystalline aggregates with elementary textures and that the 'constant stress model (CSM)' is adequate for describing the behaviour patterns of elastic properties of titanium sheet material. Directional elastic constants for the polycrystalline material were calculated from single crystal elastic constant data for HCP zirconium and (00.2) pole figure of the sample using the CSM. These directional elastic constants were used for calculating the residual stress in the three specific directions. It has also been noticed that there is substantial difference in residual stress values calculated by directional elastic constants from those calculated from bulk constants. This justifies the need to use the elastic constant calculated from the CSM.

2. Experimental procedure

2.1. Texture determination

For quantitative texture measurement Rigaku Dmax 2000 X-ray diffractometer was used. The equipment is fitted with a horizontal goniometer for texture measurement. Cu $K_\alpha(\lambda = 1.54\ \text{Å})$ radiation was used as the X-ray source (40 kV, 30 mA with Ni filter).

Pole figures of (00.2) and (10.3) were recorded and used for elastic modulus and residual stress determination respectively. To obtain the pole figures, a specimen with dimension 12 mm width × 25 mm length was cut from the tube material. The length direction was parallel to the tube RD and the tube normal (thickness) direction was parallel to the sample surface normal. To prepare specimen for reflection geometry, the tube outside surface was ground flat, polished and etched. The sample was irradiated with X-rays on this surface. In such a configuration, the tube normal direction is the center of the pole figure.

Schultz reflection technique was used [15] to get the pole figure. In reflection technique source and the detector were kept such that both were facing same side of the specimen surface. A schematic sketch is shown in Fig. 2. It uses an optical focusing system for the alignments and axis A is aligned orthogonal to the goniometer axis. α rotation refers to rotation of specimen around axis A, β rotation refers to rotation around axis B. γ oscillation represents reciprocating motion in the specimen plane which is at an angle of 45° with respect to axis A.

The X-ray diffraction data were collected in the range of tilt angle from 20° to 90°. The rotation and tilt angles were coupled in such a way that for every tilt of 5° about tube RD rotation of 360° about tube normal direction was given to the sample. The goniometer was aligned such that the Bragg diffraction condition for (10.3) plane was always maintained.

The raw data were processed for smoothening and background elimination. Also the necessary slits sizes (divergence, scattering and receiving) for this system to get optimum X-ray intensity were standardised. The processed data were plotted as stereographic projection called pole figure showing the preferred orientation of a given plane in the tube rolling and tangential directions.

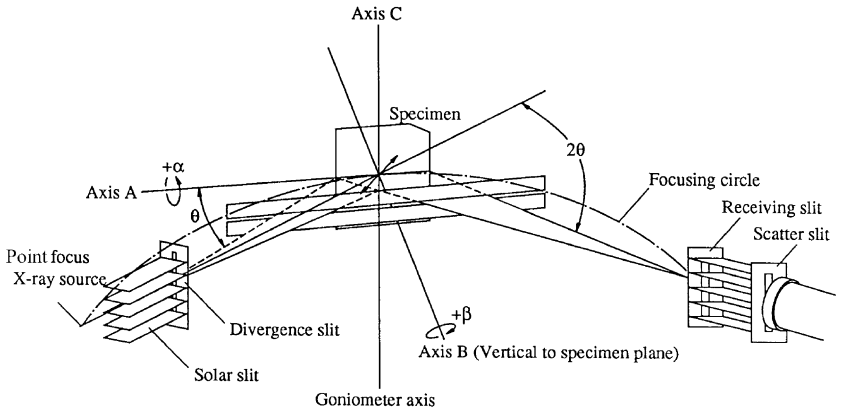

Fig. 2. Functional diagram of Schultz reflection geometry.

The equipment is fully automated using a microprocessor-controlled goniometer along with the driver and processing softwares to handle above operations and to carry out necessary data processing.

2.2. Residual stress measurement

2.2.1. Equipment

The residual stress was measured using the Stress Tech X-Stress 3000 equipment. The equipment consists of a goniometer with an X-ray source and a compact high voltage cum cooling system. The probe used was Ti Kα X-ray radiation, with two position sensitive detectors for obtaining the full X-ray diffracted peak in one exposure. The goniometer is capable of giving inclination, rotation and vertical movements. Fig. 1 gives the functional diagram of the measurement principle. As seen (case 'A') in stress free sample, with variation in inclination angle (ψ) the d-spacing will be constant. When stress is present (case 'B') the d-spacing varies as d_i in the figure.

2.2.2. Modified procedure for textured material

The residual stress was determined for as-received material (without electro polishing); the surface finish was sufficient for the measurement of both cold-worked, and stress-relieved tubes (Table 1). For zirconium, (10.3) plane ($2\theta = 139.82°$ with Ti Kα) was taken for the measurements. A minimum of five inclination angles (in each positive and negative) is required to get good correlation. For calibration purposes, a stress free zirconium powder sample was used.

In the case of textured materials for some specific combination of ϕ- and ψ-values, we get very high intensity in one of the detectors and low in the other. The basis of the stress measurement is precise determination of the peak position. For cases where we get lower intensity it is very difficult to find the exact position of the peak maxima. The following procedures have been used to reduce the error.

(a) Find specific combination of ϕs and ψs for which the height and nature of the intensity peaks are similar

Table 1
Procedure adopted for residual stress determination of textured Zr–2.5%Nb alloy pressure tubes

(1) Calibration of the measurement distance (between collemeter tip and sample surface) was performed with zirconium powder sample using X-ray with titanium target. The stress measured in the powder sample was nearly zero.
(2) Tube samples were positioned such that the X-ray collimator tip was at the top of the curved surface.
(3) Detectors are set for the exact Bragg angle $2\theta = 139.8°$ for the plane (10.3).
(4) Selecting rotation angle ϕ as 0°, 70° and 90° based on texture pole figure.
(5) Selecting inclination angle ψ at nine positions at equal intervals between $\pm 45°$ from pole figure.
(6) Data for young's modulus and Poisson's ratio, calculated using 'constant stress model'. Lattice parameters for zirconium, wavelength (λ) of the Ti from JCPDS.
(7) Measurement with exposure time at each ψ as 50 s, use the directional elastic constants (as calculated above) for the chosen rotation angles.
(8) Calculation of principal stresses.
(9) Calculation of compete stress tensors by Hauk-Dolle method.

Table 2
Directional elastic constants of polycrystalline material

Elastic constants	Directions		
	RD	70° to RD	TD
Young's modulus, E (GPa)	98.79	94.65	99.25
Poisson's ratio (v)	0.258	0.293	0.259

in both the detectors. Disable inclination angles where variations are pronounced.

(b) Calculate the directional elastic constant used for the bulk polycrystalline samples (Table 2) using the CSM [5] given in Appendix A.

In the present study, the orientations of the different sets of planes, on which lattice strain was measured, were indexed on a Wulff net. For the interpretation of the effect of crystallographic texture on the peak intensity, the corresponding pole figures were superimposed with peak intensity of stress measurements as shown in Figs. 3–5 for all the samples. It is seen that the φ directions selected for the measurement of stress are nearly texture independent. Hence the error in the reported stress values is minimum.

3. Results and discussion

The elastic constants, calculated for the three stress measurement directions, are given in Table 2. The measured stresses in the three directions are given in Table 3. The Dolle–Hauk [17] method was used for determination of full stress distribution (normal, shear in the three orthogonal directions). The stress tensor calculated using the Hauk–Dolle method described in Appendix B is given in Table 4. The principal stresses and directions calculated from the measured stresses are given in Table 5. For the comparison purpose principal stresses are calculated both with directional and bulk elastic constant. The bulk elastic constants are the standard characteristic elastic modulus values of Zr–2.5Nb alloy without any texture.

As reported by Gazzara [3], texture independent paths for residual stress can be found by superimposing the angles used for residual stress measurement on the pole figure. There are certain α (where $\alpha = 180° - 2\theta$) values for which the line drawn with varying ψ-values goes through almost uniform intensity region. For these αs the measurement of residual stress bears a linear correlation between d and $\sin^2\psi$ as the intensity peaks are high and uniform, it increases the accuracy level in determination of $\Delta 2\theta$ and hence d. In the present case the near texture independent directions were selected and the stress were calculated using the direction dependent elastic constants calculated from the crystal orientation. Figs. 3–5 shows the pole figure for the (10.3) pole superimposed with the X-ray peak intensity obtained from the residual stress measurement for all the samples. The three selected measuring directions i.e. 0°, 70° and 90° are near texture independent for both the detectors. Use of inclination angles beyond 45° leads to pronounced texture effect with low intensity peaks. Intensity difference between the two detectors was >25 units when measured along undesirable angles e.g., $\phi = 40°$. The procedure used for residual stress measurement of textured Zr–2.5Nb material is given in Table 1.

Peak maxima could be more precisely determined in case of sharp peaks than the broader ones and this gives rise to more accurate determination of residual stresses. In the present study, the peaks are sharper i.e. lower full width half maxima (FWHM) in case of the

Table 3
Measured surface residual stresses (in Mpa)

Angle of rotation (ϕ)	As-pilgered	Autoclaved
0°	-155.0 ± 20.9	13.7 ± 9.0
70°	-56.8 ± 30.9	-26.4 ± 9.8
90°	-41.8 ± 25.6	-35.3 ± 9.0

Table 4
Tensor components calculated by Hauk–Dolle method (in MPa)

Stress components	As-pilgered	Autoclaved
σ_{11}	-114.0 ± 15.8	10.4 ± 6.8
σ_{22}	-40.2 ± 7.0	-33.8 ± 3.7
σ_{33}	0.0 ± 0.0	0.0 ± 0.0
σ_{12}	0.0 ± 0.0	0.0 ± 0.0
σ_{13}	8.0 ± 2.1	-7.3 ± 1.2
σ_{23}	13.7 ± 9.4	18.7 ± 1.8

Table 5
Calculation of principal stresses and directions (in MPa)

Stress values and direction	With directional elastic constants		With bulk elastic constants	
	As-pilgered	Autoclaved	As-pilgered	Autoclaved
$\sigma 1$	−41.73	14.20	−35.06	13.34
$\sigma 2$	−155.07	−35.3	−118.2	−31.26
ϕ (°)	−2.4325	−16.38	−76	−13

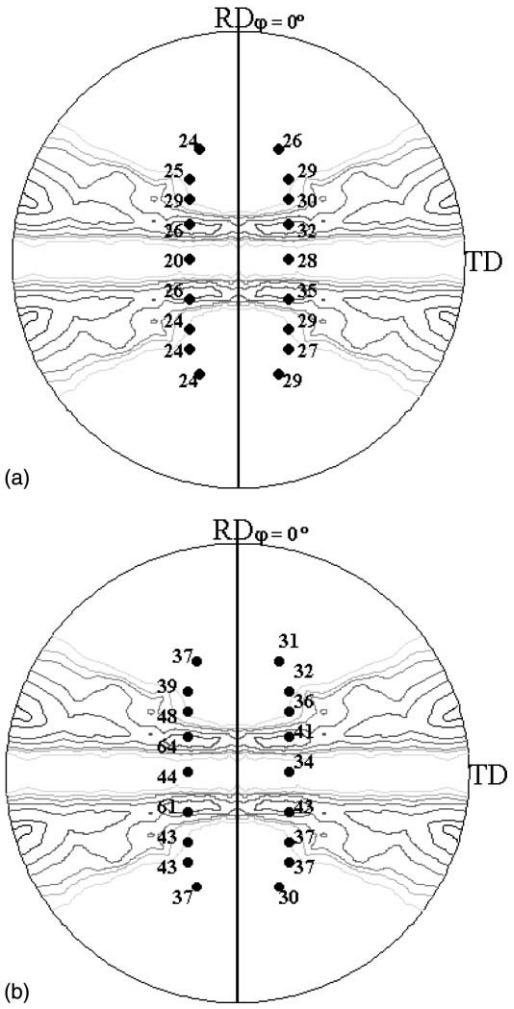

Fig. 3. Intensity of peaks during residual stress superimposed on (10.3) pole figure for $\phi = 0°$ (a) As-pilgered sample and (b) Autoclaved sample. Scale of intensity levels: see Fig. 5.

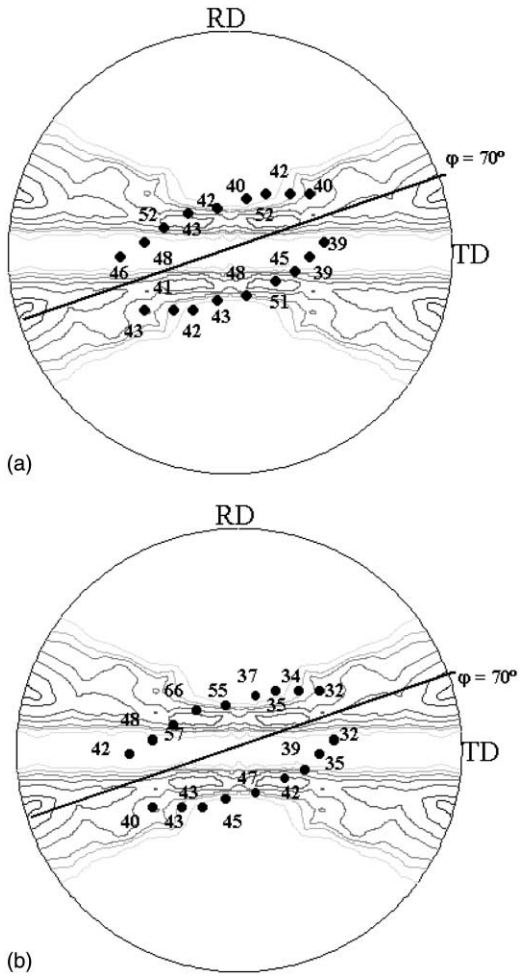

Fig. 4. Intensity of peaks during residual stress superimposed on (10.3) pole figure for $\phi = 70°$ (a) as-pilgered sample and (b) autoclaved sample. Scale of intensity levels: see Fig. 5.

stress-relieved materials as shown in Table 6. Hence, stresses calculated for autoclaved material are more accurate.

The stress is highest and compressive in nature along RD of the as cold-worked tube. In transverse direction (TD), the stress is low and still compressive in nature. In the autoclaved tube stress largely reduces in the RD and the component is tensile and very low in magnitude. Also in this case stresses are nearly symmetric in all the directions.

Principal stress direction in both the cases are along with the tube symmetric axis. There is a difference of 20% in the major principal stress values calculated using bulk elastic constant and the directional elastic constants obtained using the CSM (Table 5).

A full tensor analysis is done using Hauk-Dolle method [17]. The stress values show that the normal stress directions exactly match with the sample directions, i.e., RD is parallel to σ_{11} and TD to σ_{22} as the principal stresses. In the cold-worked tube, normal stresses, especially σ_{11} are high and compressive in nature, after autoclaving σ_{11} changes to a low tensile value. Due to low depth of penetration of the beam measurement was done on a very thin surface layer hence σ_{33} is turnout to be '0' in both the cases. Shear stress values are also very low in pilgered and autoclaved tubes. The yield strength (YS) of this material is ~385 MPa, hence the normal and shear stress determined in this material are less than 10% of the YS.

The only approximation adopted in the whole study is in the constant stress model used for calculation of directional elastic constants. The model assumes that the grains within a polycrystalline aggregate are stressed uniformly, which is not completely valid, for there must

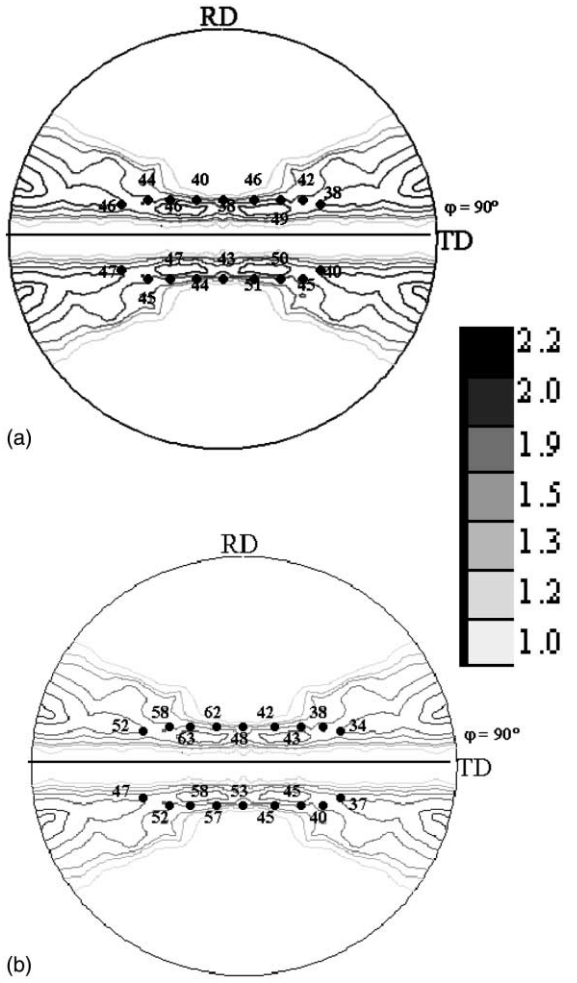

Fig. 5. Intensity of peaks during esidual stress superimposed on (10.3) pole figure for $\phi = 90°$ (a) as-pilgered sample and (b) autoclaved sample.

Table 6
Full width half maxima (FWHM) of peaks in as cold-worked and stress-relieved samples

Direction of measurement	Full width half maxima (nm)	
	As-pilgered	Autoclaved
RD	3.46	1.38
70° to RD	3.19	1.35
TD	2.76	1.36

be a discontinuity in stress at or near the grain boundary of adjacent grains that have different orientations. But error from this source decreases with the development of a strong texture due to smaller misorientation between the adjacent grains. As in the present case the texture is very strong this limitation is not applicable.

4. Conclusions

Accurate measurement of X-ray residual stress in the textured Zr–2.5Nb requires a thorough knowledge of texture in the material. The correct measurement directions are selected from the pole figure of the measuring plane (10.3). The 0°, 70° and 90° to RD are the texture independent direction for this material. The direction dependent elastic constants are deduced from the single crystal data with the (00.2) pole figure. After measuring the stress in three directions, the full tensor and the principal stresses were evaluated. Cold-worked material had the principal residual stress components (compressive in nature) along rolling and transverse directions of the tube, autoclaving leads to reduction of stress to less than 10% of YS, and reorientation of the stress components. Shear stresses are found to be very low in both the cases.

Acknowledgements

The authors acknowledge the useful discussions with Dr C. Gangluy, Chief Executive Nuclear Fuel Complex, Hyderabad and his guidance during the course of this work. Authors also wish to thank S.C. Jain, Deputy Chief Executive for his encouragement during the work.

Appendix A. Calculation of directional elastic constants using 'constant stress model' [5]

The constant stress model uses two matrices namely I & II for determining the directional elastic constants, which transforms the orientation of polycrystalline texture in terms of specimen axis. The matrices are defined as follows:

Matrix-I

	X	Y	Z
X'	$\cos\omega\sin\beta$	$\cos\beta$	$\sin\omega\sin\beta$
Y'	$\cos\omega\cos\beta$	$-\sin\beta$	$\sin\omega\cos\beta$
Z'	$-\sin\omega$	0	$\cos\omega$

Matrix-II

	X	Y	Z
X'	I_1	m_1	n_1
Y'	I_2	m_2	n_2
Z'	I_3	m_3	n_3

Here, β is the angle between the RD and the specimen axis, ω is the angle between the basal pole and the tube normal. X' is the RD, Y' is the transverse direction and Z' is the tube normal direction. X, Y and Z are the

Table 7
Elastic constants of HCP zirconium single crystal

Elastic stiffness	10^5 MPa	Elastic compliances	10^{-5} MPa^{-1}
C_{11}	1.434	S_{11}	1.012
C_{12}	0.728	S_{12}	−0.404
C_{13}	0.653	S_{13}	−0.241
C_{33}	1.648	S_{33}	0.798
C_{44}	0.320	S_{44}	3.125

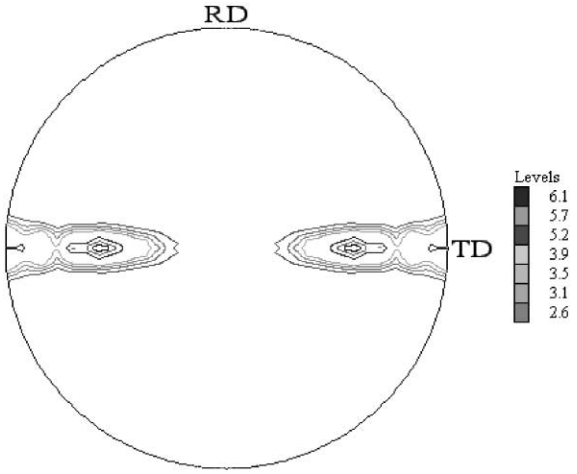

Fig. 6. (00.2) Pole figure of pilgered and autoclaved tube.

coordinates of texture and Z coincides with the maximum intensity of the basal pole.

The single crystal elastic constants given in Table 7 [16] are used to calculate the values of the directional elastic constants, using the (00.2) pole figure (Fig. 6) and the following equations. The results are reported in Table 2.

For Young's modulus,

$$1/E = S'_{11} = S_{33} + (1-n_1^2)(S_{11}-S_{33}) - n_1^2(1-n_1^2)(S_{11}+S_{33}-2S_{13}-S_{44}). \quad (A.1)$$

For Poisson's ratio,

$$\begin{aligned} v &= S'_{12}/S'_{11} \\ &= -\{S_{13}+n_3^2(S_{12}-S_{13})+n_1^2n_2^2(S_{11}+S_{33}-2S_{13}-S_{44})\} \\ &\quad /\{S_{33}+(1-n_1^2)(S_{11}-S_{33})-n_1^2(1-n_1^2) \\ &\quad \times (S_{11}+S_{33}-2S_{13}-S_{44})\}. \end{aligned} \quad (A.2)$$

Appendix B. Calculation of stress tensor based on Hauk–Dolle method [17]

In Fig. 7, $\underline{S}_i$ defines the surface co-ordinate system of the specimen with $\underline{S}_1$ and $\underline{S}_2$ lying in the sample surface.

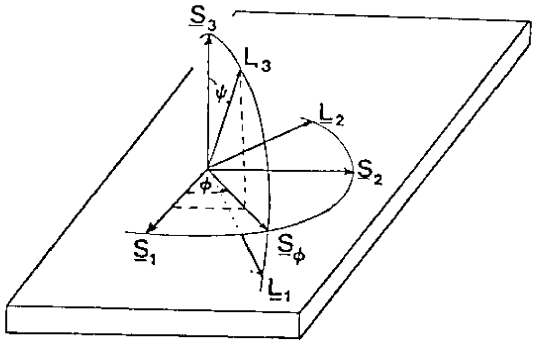

Fig. 7. The definition of the laboratory coordinate system $\underline{L}_i$, sample coordinate system $\underline{S}_i$, and the angles ϕ, ψ.

The laboratory system $\underline{L}_i$ is defined such that $\underline{L}_3$ is in the direction normal to the family of planes (hkl) whose spacing is measured by X-rays. $\underline{L}_2$ is in the plane defined by $\underline{S}_1$ and $\underline{S}_2$ and makes an angle ϕ with $\underline{S}_2$.

The fundamental equation to determine strain by Dolle-Hauk method is

$$\begin{aligned} (\varepsilon'_{33})\phi\psi &= \varepsilon_{11}\cos^2\phi\sin^2\psi + \varepsilon_{12}\sin 2\phi\sin^2\psi \\ &\quad + \varepsilon_{22}\sin^2\phi\sin^2\psi + \varepsilon_{33}\cos^2\psi \\ &\quad + \varepsilon_{13}\cos\phi\sin 2\psi + \varepsilon_{33}\sin\phi\sin 2\psi. \end{aligned} \quad (B.1)$$

It is a linear equation with six unknowns, ε_{11}, ε_{12}, ε_{22}, ε_{33}, ε_{13}, ε_{23}, and may be solved if $d_{\phi\psi}$ is measured at minimum six independent directions separately. In practice, measurement was done at more points to improve the accuracy. The solution of the Eq. (B.1) was done by Hauk–Dolle method as described below:

Two parameters a_1 and a_2 was defined as

$$\begin{aligned} a_1 &= 1/2[\varepsilon_{\phi\psi+}+\varepsilon_{\phi\psi-}] \\ &= \{(d_{\phi\psi+}+d_{\phi\psi-})/2d_o - 1\} \\ &= \{\varepsilon_{11}\cos^2\phi + \varepsilon_{12}\sin 2\phi + \varepsilon_{22}\sin^2\phi - \varepsilon_{33}\} \\ &\quad \sin^2\psi + \varepsilon_{33}, \end{aligned} \quad (B.2)$$

$$\begin{aligned} a_2 &= 1/2[\varepsilon_{\phi\psi+}-\varepsilon_{\phi\psi-}] = (d_{\phi\psi+}-d_{\phi\psi-})/2d_o \\ &= \{\varepsilon_{13}\cos\phi + \varepsilon_{23}\sin\phi\}\sin|2\psi|, \end{aligned} \quad (B.3)$$

where, $\psi_- = (-1)\psi_+$ and $\sin 2\psi_+ - \sin 2\psi_- = 2\sin|2\psi|$.

Eq. (B.2) predicts a linear variation of a_1 with $\sin^2\psi$ with the slope and intercept given by

$$(m_\phi)_{a1} = \varepsilon_{11}\cos^2\phi + \varepsilon_{12}\sin 2\phi + \varepsilon_{22}\sin^2\phi - \varepsilon_{33}, \quad (B.4)$$

$$(I)_{a1} = \varepsilon_{33}. \quad (B.5)$$

Similarly, a_2 varies linearly with $\sin|2\psi|$. The slope in this case is,

$$(m_\phi)_{a2} = \varepsilon_{13}\cos\phi + \varepsilon_{23}\sin\phi. \quad \text{(B.6)}$$

Thus, if $d_{\phi\psi}$ data is obtained over a range $\pm\psi$ at three ϕ tilts (0°, 45°, 90°), and a_1 vs. $\sin^2\psi$ and a_2 vs. $\sin|2\psi|$ are plotted for all ψ, the quantities $\varepsilon_{11} - \varepsilon_{33}$, $1/2(\varepsilon_{11} + 2\varepsilon_{12} + \varepsilon_{22} - 2\varepsilon_{33})$ and $(\varepsilon_{22} - \varepsilon_{33})$ could be obtained from Eq. (B.4) (at $\phi = 0°$, 45° and 90° respectively). The intercept of a_1 vs. $\sin^2\psi$ is equal to ε_{33} at all ψ tilt from Eq. (B.5). Similarly, the slope of a_2 vs. $\sin|2\psi|$ for $\phi = 0°$, 90° calculates the quantities ε_{13} and ε_{23}.

References

[1] D. Hardie, M.W. Shanahan, J. Nucl. Mater. 50 (1971) 40.
[2] R.H. Marion, J.B. Cohen, Adv. X-ray Anal. 18 (1975) 466.
[3] V. Hauk, H. Sesemann, Z. Metallkd. 67 (1978) 646.
[4] C.P. Gazzara, The Measurement of X-ray residual stress in textured cubic materials, in: Proc. Fall Mtg., SESA, Keystone, CO, 1981, p. 32.
[5] H. Dolle, J.B. Cohen, Metall. Trans. A 11A (1980) 831.
[6] P.A. Turner, C.N. Tome, Acta Metall. 42 (1994) 4143.
[7] S.R. MacEwen, C.N. Tome, in: Zirconium in the Nuclear Industry Seventh International Symposium, American Society of Testing and Materials, Philadelphia, PA, 1987, p. 631, ASTM STP 939.
[8] R. Hill, J. Mech. Phys. Solids 13 (1965) 89.
[9] J.W. Hutchinson, Proc. R. Soc. Lond. A 319 (1970) 247.
[10] J.W.L. Pang, T.M. Holden, P.A. Turner, T.E. Mason, Acta Mater. 47 (1999) 373.
[11] S.R. MacEwen, C. Tome, J. Faber Jr., Acta Metall. 37 (1989) 979.
[12] S.R. MacEwen, J. Faber Jr., A.P.L. Turner, Scr. Metall. 18 (1984) 629.
[13] J.A. Sue, Surf. Coat. Technol. 54&55 (1992) 154.
[14] A. Zarkades, F.R. Larson, in: R.I. Jaffee, N.E. Promisel (Eds.), The Science Technology and Application of Titanium, Pergamon, Oxford, 1970, p. 933.
[15] L.G. Schultz, J. Appl. Phys. 20 (1949) 741.
[16] E.S. Fisher, C.J. Renken, J. Phys. Rev. 135 (1964) A482.
[17] H. Dolle, V. Hauk, Z. Metalkd. 68 (1977) 728.